

Theoretical Study of Structure, Vibrational Frequencies, and Electronic Spectra of Polychlorinated Dibenzo-*p*-dioxins

Ivan Ljubić* and Aleksandar Sabljic

Department of Physical Chemistry, Ruđer Bošković Institute, P.O. Box 180, HR-10002, Zagreb, Republic of Croatia

Received: October 20, 2005; In Final Form: February 8, 2006

The structure, vibrational frequencies, and excited states of 2,3,7,8-tetrachloro-, 1,4,6,9-tetrachloro-, and octachlorodibenzo-*p*-dioxin (2,3,7,8-TCDD, 1,4,6,9-TCDD, and OCDD) were studied via complete active space SCF followed by the multireference second-order perturbative approach (CAS/SCF/CASPT2), as well as the time-dependent density functional theory (TD-B3LYP). The cc-pVDZ basis set and the full π -electron active spaces of 16 electrons in 14 active orbitals were employed. Whereas 2,3,7,8-TCDD assumes a planar D_{2h} minimum, 1,4,6,9-TCDD and OCDD are slightly folded exhibiting the C_{2v} symmetry. The extra stabilization due to the folding is very small. In all three isomers the highly intensive band system in the 200–240 nm region is dominated by the transitions to the 2^1B_{2u} and 3^1B_{2u} states with by far the largest oscillator strengths. The low-intensity absorptions in the 280–320 nm region can be attributed to the $1^1B_{2u} \leftarrow 1^1A_g$, with possible contribution of the vibronically allowed $2^1A_g \leftarrow 1^1A_g$ transition. Both CASPT2 and TD-B3LYP convincingly predict 1^3B_{3g} to be the lowest lying triplet state, which contradicts the experimental assignments. Calculated harmonic wavenumbers and absorption spectra agree well with the experimental data, and are sufficiently distinct to allow for an unambiguous identification of the three isomers.

Introduction

It was recognized during the 1970s that polychlorinated derivatives of dibenzo-*p*-dioxin (dioxins, PCDDs) pose a serious concern as a ubiquitous and extremely hazardous class of organic pollutants.^{1–3} Since then the incineration of domestic, industrial, and hospital waste, as well as natural combustion processes (e.g., volcanic activity), have been identified as the principal emission sources of PCDDs to the environment,^{4–6} with the main route of human exposure via food intake.⁷ Of 75 PCDD isomers, 2,3,7,8-tetrachlorodibenzo-*p*-dioxin (2,3,7,8-TCDD, Figure 1) is confirmed as the most harmful and serves as a standard in determining the Toxic Equivalency Factors (TEFs) of mixtures of polychlorinated dioxins and dibenzofurans (PCDD/PCDF), the two closely related classes of pollutants.^{8,9} Apart from its extreme acute toxicity, 2,3,7,8-TCDD is also capable of causing serious long-term effects by acting as a potent tumor promoter and teratogen,¹⁰ presumably by weakening and altering the immune and endocrine function.¹¹ It should be mentioned, however, that there still exist controversies as to the real extent of adverse effects of dioxins to humans, ensuing mainly from the fact that the susceptibility and toxic response vary hugely among different animal species.¹²

In view of the evident importance of investigations into PCDDs, the number of experimental studies on their spectroscopical properties must be considered relatively low, which is for the most part due to the extreme safety measures required for their handling. The primary goal is the design of methods for real-time monitoring, identification, and deactivation of PCDD isomers in environmental samples, in connection to which an accurate assignment of infrared (IR) and electronic absorptions becomes essential for distinguishing between their similar spectra.^{14–24} Separation of isomers by gas chromatog-

raphy (GC) followed by Fourier transform IR spectroscopy (FT-IR) produced valuable results at low microgram concentrations of PCDDs.¹⁷ High-quality IR spectra of the tetrachlorinated isomers were obtained via the matrix isolation IR (MI/FT-IR) and microdiffuse reflectance FT-IR (DRIFT) techniques.^{14,15} Gastilovich and co-workers managed to provide additional data on fundamental frequencies of symmetric modes by means of Raman spectroscopy and analysis of vibrational progressions in the phosphorescence spectra of 2,3,7,8-TCDD and 1,3,6,8-TCDD.^{22–24} Previous theoretical studies on the harmonic frequencies made use of the Hartree–Fock and density functional theory methods with basis sets of at most double- ζ quality with one set of polarization functions.^{25–29} The assignment of the IR spectra of several tetrachlorinated isomers relied on the scaled B3LYP/6-31G(d) force fields (SQM-B3LYP).²⁵ It was concluded that the achieved accuracy is sufficient to reliably distinguish between the isomers.²⁵

The approximate molecular geometries of many PCDDs, deduced from the FT-IR spectra, yielded interesting conjectures as to relations between the ground-state structure and toxicity.¹⁸ The two plausible candidates for the equilibrium geometry of the dioxin skeleton include the planar minimum (of D_{2h} symmetry in the three isomers of Figure 1) as well as the C_{2v} folded structure reminiscent of a butterfly flapping wings. Such butterfly-like folding preserves the σ_{xy} and σ_{xz} reflection planes, while only the x -axis remains 2-fold (Figure 2). The angle α closed by the two benzene rings commonly serves as a convenient measure of the molecular distortion. There are still controversies as to which type of minimum is assumed in ground and excited states, and whether specific substitution patterns may decide upon the issue.^{18,30,31}

Studies into electronic transitions of PCDDs made use of the UV absorption, low and room-temperature laser induced fluorescence (LIF), and Shpol'skii phosphorescence.^{19–24} The

* Address correspondence to this author. E-mail: iljubic@irb.hr.

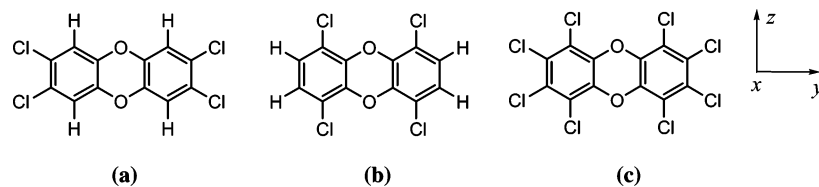


Figure 1. Three studied polychlorinated dioxins: (a) 2,3,7,8-tetrachlorodibenzo-*p*-dioxin (2,3,7,8-TCDD), (b) 1,4,6,9-tetrachlorodibenzo-*p*-dioxin (1,4,6,9-TCDD), and (c) octachlorodibenzo-*p*-dioxin (OCDD). The molecule-fixed coordinate system is oriented in line with the IUPAC conventions.¹³

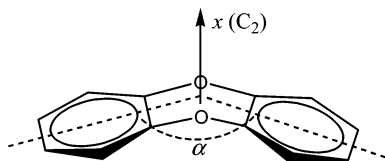


Figure 2. The butterfly conformation of the dioxin skeleton.

latter two techniques enabled assignment of the lowest singlet and triplet states, which belong to the 300 nm and higher region of the spectrum.^{19,21–23} As to the much more intense band system spanning the 200–240 nm range, the peak absorbance and emission wavelengths were reported in the region, but no assignment was attempted.^{19,20}

Because practically nothing beyond that is known on the nature and ordering of electronic transitions in PCDDs, theoretical studies into the fundamental electronic properties gain a high importance. The previous calculations employed mainly the semiempirical based configuration interaction in the space of singly excited configurations (CIS),^{23,24,30b} although the *ab initio* CIS method was also tested.^{31,32} The excitation energies resulting from semiempirical CNDO and INDO-CIS required large redshifts, in the range of 5000–7000 cm^{-1} , to bring them in the vicinity of experimental absorptions.^{23,24} The CIS/6-31G(d,p) method proved equally unsatisfactory, resulting on average by 9000 cm^{-1} too high excitation energies for the $S_1 \leftarrow S_0$ transition in the parent DD and several investigated PCDDs.^{31,32} Because such discrepancies are on the order of a large portion of the recorded UV spectral range, the semiempirical and *ab initio* CIS excitation energies, as well as the corresponding ordering of the electron states, are for that matter highly unreliable.

A logical step forward toward a more reliable prediction of the excitation energies and assignment of the electronic spectra calls for the correlated multiconfigurational treatments. Such a theoretical study has not been carried out thus far. Multireference CI (MR-CI) treatments being presently unaffordable for systems of similar size, a feasible choice is the second-order perturbation theory based on the complete active space SCF reference wave function (CASSCF/CASPT2).³³ Throughout the past decade the CASPT2 method has been established as a remarkably successful tool in rationalizing the electronic spectra of a wide variety of molecules.³⁴ An interesting alternative is commonly provided by the time dependent DFT (TD-DFT) approaches.³⁵ In the present paper, the CASPT2 and TD-DFT methods are employed in investigating the molecular structure, harmonic vibrational frequencies, and excited electronic states of three PCDDs: 2,3,7,8-TCDD, 1,4,6,9-TCDD, and OCDD (Figure 1).

Computational Methods

The stationary geometries and the harmonic vibrational wavenumbers of the three polychlorinated dioxins were calculated via the multiconfigurational complete active space SCF (CASSCF) method,³⁶ as well as the density functional theory based upon the Becke styled hybrid functional B3LYP.³⁷ In the multiconfigurational calculations we used the active spaces of 16 electrons distributed among 14 active orbitals. Near equi-

librium geometries these active spaces tended to be completely analogous to that used in the parent DD,³⁸ although with the three chlorinated derivatives extra care had to be taken to avoid an excessive involvement of the out-of-plane chlorine lone pairs, which are only of a limited interest. Eventually, their participation was made negligible, and the active space was essentially built of the π orbitals on the carbon atoms and the oxygen lone pairs. A pictorial representation (using MOLDE³⁹) of a typical ground-state active space is available in the Supporting Information.

Because of the size of the problem, the CASSCF geometric optimizations were mainly conducted by constraining the structures to the D_{2h} point group symmetry. Also manageable was the C_{2v} point symmetry, whereby the planar geometries were tested for the possibility of a butterfly-like relaxation. Within the $D_{2h}(C_{2v})$ point groups, using the molecule fixed coordinate frame as in Figure 1, the (16,14) active space consisted of the $3b_{1g}(b_2)$, $4b_{2g}(b_1)$, $4b_{3u}(a_1)$, and $3a_u(a_2)$ molecular orbitals (MOs). Thus, the $\pi-\pi^*$ states belong to the A_g , B_{3g} , B_{1u} , and B_{2u} symmetry species, whereas participation of one σ and one π type orbital may give rise to the A_u , B_{1g} , B_{2g} , and B_{3u} states. The CAS state averaged (CAS-SA) calculations⁴⁰ were performed over a few equally weighted lowest roots (2 to 4 of them) in the A_g , B_{3g} , B_{1u} , and B_{2u} symmetries. The dynamical electron correlation was accounted for via the single state CASPT2 calculations³³ with the calculated CASSCF roots as the zeroth order references. The CASPT2 energy differences were used in calculating the vertical and adiabatic excitation energies. The vertical energies were compared to those obtained via the time-dependent density functional theory approach (TD-B3LYP). The nature of the (16,14) active space limited the application of the CASSCF/CASPT2 approach to the low-lying valence $\pi-\pi^*$ states, while TD-B3LYP contributed several additional states.

Unlike the situation with DD,³⁸ in the chlorinated derivatives use of the level shifting technique (CASPT2-LS)³⁴ proved necessary to correct the second-order energies for the presence of near-singularities (intruders). Their emergence was expected on account of the excitations from the near-lying out-of-plane chlorine lone pairs. Here we opted for the imaginary level shift (ILS) technique as formulated by Forsberg and Malmqvist,⁴¹ because it proved quite efficient in the calculations on the $n-\pi^*$ states of DD.³⁸ This shifting technique, unlike the real, does not deal with the intruders by merely shifting them up the real axis,⁴² which may cause new singularities, but rather moving them away from the axis.⁴¹ As with the $n-\pi^*$ states of DD,³⁸ the ILS parameter of 0.20 hartree proved efficient and was applied throughout. It was observed that, while successfully solving the problem of intruders in all the affected states, the applied parameter did not significantly modify the remaining excitation energies, shifting them on average by ± 0.02 eV. The weights of the CASSCF references in the first order wave function equaled 0.56 and 0.50 for the ground state TCDDs and OCDD, respectively, without a single larger contribution to the second order energy. This convinced us that similar

magnitudes of reference weights are physically plausible within the used computational approach. The ILS technique increased the weights of the intruder affected references to within 5% of those of the ground state, thus rendering the second-order approach sensible.

Combined with ILS, a modification of the zeroth-order Hamiltonian, designated g_2 , was applied to mitigate a systematic error of overestimation of the stability of open shells in CASPT2.⁴³ The performance of the CASPT2(g_2)-ILS technique, already established in the studies on DD,³⁸ was tested against a newly developed CASPT2-IPEA approach.⁴⁴ In this approach the diagonal elements of the Fock operator are modified by a suitable IPEA level shift weighted by the corresponding diagonal element, whereby the energy denominators assume approximate values of electron affinity (EA) or ionization potential (IP), depending on whether the excitation is into or from a partially occupied orbital.⁴⁴ Upon testing a range of IPEA level shift values, it was observed that with the recommended value of 0.25 hartree clearly overestimated excitation energies result. Consequently, a value of 0.10 hartree was adopted, combined with the imaginary shift of 0.20 hartree necessary for removing a persistent intruder in the B_{2u} state of all three isomers.

In all calculations the standard Dunning's correlation consistent cc-pVDZ basis set⁴⁵ was used, contracted to (4s3p1d) on Cl, (3s2p1d) on C and O, and (2s1p) on the H atom. This amounts to 288 and 340 basis functions in TCDDs and OCDD, respectively. As the cc-pVDZ set is inadequate for describing core correlation, all CASPT2 calculations were performed with the inner shells of the O, C, and Cl atoms frozen. Presently, larger or more flexible basis sets prove prohibitive in calculations on this scale. Even so, the use of the cc-pVDZ set and an analogous (16,14) active space in DD proved rather encouraging.³⁸

The multireference based calculations were performed with MOLCAS 6.2,⁴⁶ and the time-dependent DFT with the Gaussian 03 quantum-chemical suite.⁴⁷ The CASSCF transition dipole moments (TDMs) in length representation were calculated employing the RASSI module of MOLCAS.⁴⁸ The oscillator strengths f were calculated from the CASSCF TDMs and the CASPT2 vertical excitation energies ΔE (in hartrees) according to

$$f = \frac{2}{3} (\text{TDM})^2 \Delta E \quad (1)$$

Results and Discussion

A. Geometrical Parameters. Geometrical parameters of the ground states of 2,3,7,8-TCDD, 1,4,6,9-TCDD, and OCDD, as well as the parameters of the lowest singlet and triplet $\pi-\pi^*$ excited states in each symmetry, are shown in Table 1.

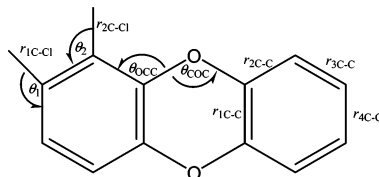
A.1. Ground-State Geometries. In 2,3,7,8-TCDD the changes in molecular geometry induced by the chlorine substitution are only minor relative to DD,³⁸ the most notable ones being shortening of r_{2C-C} and r_{C-O} by 0.005 and 0.002 Å, respectively. In 1,4,6,9-TCDD and OCDD r_{C-O} is more shortened, by 0.007 and 0.008 Å, respectively, and the C–O–C angle is increased by approximately 1°. The C–C distances in 1,4,6,9-TCDD are more alike, spanning the range of only 0.005 Å, with r_{4C-C} becoming the shortest (1.392 Å) and r_{1C-C} the longest (1.397 Å), whereas in OCDD r_{3C-C} and r_{4C-C} are notably more elongated. The described occurrences can be explained by the repulsive interactions between the vicinal O and Cl atoms, and in particular between the vicinal Cl atoms in OCDD. The overall trends in OCDD are in accord with the experiment,⁵⁰ although both CASSCF and B3LYP predict r_{3C-C} to be somewhat more

extended (Table 1). In 2,3,7,8-TCDD both methods correctly predict the patterns in the C–C bond lengths with r_{2C-C} being ~ 0.1 Å shorter than the remaining C–C distances, which agrees well with the trends from the X-ray data.⁴⁹ The X-ray structure reported for 2,3,7,8-TCDD is essentially planar,⁴⁹ whereas in OCDD the authors allowed for a possibility of small deviations from planarity.⁵⁰

The CASSCF method predicts on average 0.018 Å too short C–O bonds, whereas the C–C and C–Cl bonds are on average 0.011 Å too long compared to the X-ray parameters.^{49,50} On the other hand, the B3LYP method results in the C–O bond lengths, which are in excellent agreement with the experiment, whereas the C–C and in particular C–Cl bonds are elongated on average by 0.02 Å, even more than the CASSCF values. As to the bonds of the dibenzo-*p*-dioxin skeleton, the CASSCF trends are comparable to those seen in benzene⁵¹—the two opposing effects, which partially cancel each other out, result in relatively favorable parameters overall. These are, on one side, the tendency toward elongating the explicitly correlated π component of the bonds by generally giving too large a weight to the antibonding orbitals, and on the other, the tendency toward shortening the uncorrelated σ component. Likewise, the CASSCF C–O bond lengths remain considerably underestimated because of the lack of the active orbitals to effectively correlate the out-of-plane lone pairs on the O atoms. The error of overestimating the C–Cl distance in Cl-substituted benzenes regardless of the basis set size appears typical of the SCF and B3LYP treatments, judging from the same discrepancy visible in chlorobenzene.⁵²

The CASSCF optimizations of 1,4,6,9-TCDD and OCDD constrained to the D_{2h} symmetry resulted in stationary structures that were subsequently confirmed as the first-order saddle points. In both compounds the imaginary wavenumbers corresponded to the butterfly folding mode, which prompted us to search for the C_{2v} butterfly minima. From very small absolute values of the imaginary wavenumbers (2.5 and 3.0 cm^{-1} for 1,4,6,9-TCDD and OCDD, respectively) only slight deviations from the planarity were expected, which would in turn result in only a small overall stabilization. The parameters in folded geometries (Table 1) indeed differ negligibly from the D_{2h} saddle points and the folding angles α and β are close to 180° (Table 2). The relaxation induces dipole moments of 0.387 D in 1,4,6,9-TCDD and only 0.004 D in OCDD, and the wavenumbers of the butterfly folding modes become real, equaling 15 cm^{-1} (7 cm^{-1}) in 1,4,6,9-TCDD (OCDD). At the CASSCF level the folded structures are stabilized by only 0.03 kJ mol^{-1} (0.06 kJ mol^{-1}) relative to the planar ones. Interestingly, this trend is maintained at the correlated CASPT2 level, with both stabilization energies approaching 0.1 kJ mol^{-1} . Similar remarkably small barriers to the butterfly folding are typical of the dioxin skeleton, as was also observed in DD.³⁸ Thus the relaxation to the C_{2v} minima is expected to have an almost negligible effect on the CASPT2 excitation energies and oscillator strengths. These effects were probed by means of the cheaper TD-B3LYP approach (Section C).

The principal driving force behind the relaxation is the decrease in repulsion between the in-plane lone pairs of the vicinal O and Cl atoms. Their mutual distance in the process is increased to 2.937 Å (by 0.007 Å), which is still considerably less than the sum of their van der Waals radii ($r_{vdW}(\text{O}) = 1.4$ Å; $r_{vdW}(\text{Cl}) = 1.8$ Å). Because any departure from the planarity takes place at the expense of a less pronounced stabilization via the π electron delocalization, the final extent of folding reflects a compromise between the stabilizing and repulsive

TABLE 1: Geometric Parameters of the 1^1A_g Ground States of 2,3,7,8-TCDD, 1,4,6,9-TCDD, and OCDD at the CASSCF(16,14)/cc-pVDZ and B3LYP/cc-pVDZ Levels

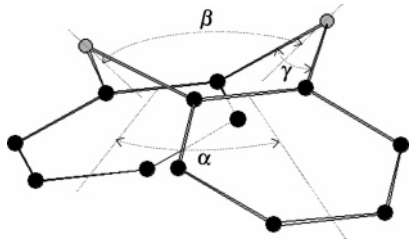
2,3,7,8-TCDD											
1^1A_g	r_{C-O}	r_{1C-C}	r_{2C-C}	r_{3C-C}	r_{4C-C}	r_{1C-Cl}	θ_{COC}	θ_{OCC}	θ_1		
CASSCF	1.361	1.395	1.387	1.397	1.397	1.737	116.6	118.2	121.9		
B3LYP	1.379	1.401	1.389	1.400	1.401	1.746	115.9	117.9	121.7		
exptl ^a	1.378	1.387	1.376	1.382	1.388	1.728	115.6	117.6	121.2		
$\pi-\pi^*$											
1^1B_{3g}	1.326	1.427	1.410	1.372	1.451	1.737	119.4	119.9	120.8		
1^1B_{2u}	1.351	1.407	1.409	1.413	1.417	1.732	117.8	118.2	121.6		
1^1B_{1u}	1.337	1.434	1.401	1.404	1.471	1.727	120.0	119.4	121.1		
1^3A_g	1.349	1.410	1.405	1.409	1.409	1.733	117.4	117.9	121.5		
1^3B_{3g}	1.345	1.437	1.397	1.389	1.452	1.733	118.9	119.4	121.0		
1^3B_{2u}	1.347	1.413	1.404	1.412	1.408	1.733	118.7	118.6	121.6		
1^3B_{1u}	1.363	1.381	1.418	1.428	1.388	1.734	115.2	117.1	122.3		
1,4,6,9-TCDD											
1^1A_g	r_{C-O}	r_{1C-C}	r_{2C-C}	r_{3C-C}	r_{4C-C}	r_{2C-Cl}	θ_{COC}	θ_{OCC}	θ_2		
CASSCF	1.356	1.397	1.393	1.395	1.392	1.736	117.7	119.0	120.0		
folded	1.356	1.397	1.392	1.396	1.392	1.736	117.4	119.3	120.0		
B3LYP	1.374	1.402	1.397	1.398	1.392	1.746	117.2	116.9	120.4		
$\pi-\pi^*$											
1^1B_{3g}	1.321	1.432	1.417	1.369	1.441	1.737	120.5	120.8	121.1		
1^1B_{2u}	1.346	1.413	1.414	1.411	1.411	1.731	118.7	119.3	120.3		
1^1B_{1u}	1.332	1.440	1.406	1.403	1.462	1.733	121.0	120.5	120.2		
1^3A_g	1.345	1.417	1.410	1.409	1.404	1.733	118.3	119.0	120.5		
1^3B_{3g}	1.338	1.442	1.404	1.385	1.443	1.736	120.0	120.4	120.4		
1^3B_{2u}	1.343	1.421	1.408	1.412	1.402	1.732	119.4	119.7	120.4		
1^3B_{1u}	1.358	1.383	1.424	1.426	1.383	1.727	116.2	118.0	120.0		
OCDD											
1^1A_g	r_{C-O}	r_{1C-C}	r_{2C-C}	r_{3C-C}	r_{4C-C}	r_{1C-Cl}	r_{2C-Cl}	θ_{COC}	θ_{OCC}	θ_1	θ_2
CASSCF	1.355	1.391	1.393	1.403	1.403	1.729	1.727	117.8	118.5	119.7	118.4
folded	1.355	1.391	1.393	1.403	1.403	1.729	1.727	117.4	118.9	119.7	118.5
B3LYP	1.374	1.396	1.397	1.408	1.405	1.737	1.736	116.8	118.1	120.4	121.7
exptl ^b	1.374	1.383	1.382	1.386	1.392	1.717	1.718	115.9	117.5	119.5	118.9
$\pi-\pi^*$											
1^1B_{3g}	1.320	1.424	1.417	1.375	1.458	1.728	1.727	120.4	120.2	119.4	122.7
1^1B_{2u}	1.345	1.406	1.413	1.420	1.423	1.724	1.722	118.9	118.7	120.2	122.2
1^1B_{1u}	1.330	1.434	1.406	1.410	1.477	1.719	1.724	121.1	119.9	119.7	121.9
1^3A_g	1.345	1.407	1.411	1.416	1.418	1.724	1.724	118.3	118.4	120.2	122.4
1^3B_{3g}	1.337	1.435	1.402	1.392	1.460	1.724	1.727	120.1	119.8	119.5	122.1
1^3B_{2u}	1.342	1.412	1.408	1.419	1.415	1.724	1.724	119.5	119.0	120.3	122.3
1^3B_{1u}	1.357	1.376	1.424	1.436	1.391	1.726	1.718	116.2	117.4	120.9	121.9

^a Experimental geometry from crystallographic data (ref 49). ^b Experimental geometry from crystallographic data (ref 50).

effects. Thus, despite the large CASSCF active space, which correlates all the π electrons, the folding may be regarded as an artifact of the missing dynamical correlation contributions, whereby the energy gains via electron delocalization are underestimated, and the purely electrostatic repulsion between the O and Cl atoms is given more weight. HF/cc-pVDZ likewise yields a bent minimum, whereas planar D_{2h} minima result at the B3LYP/cc-pVDZ and MP2/cc-pVDZ levels, all confirmed by the harmonic wavenumbers analysis. Regarding minimum conformations, similar discrepancies between different quantum chemical approaches were discovered several times in the past.⁵³ We believe that a correlated multiconfigurational method accompanied by a larger basis set is required for a definitive answer on correct conformations of the 1,4,6,9-TCDD and OCDD minima, because the final result reflects a very delicate balance between the two opposing effects.

The attempts at rationalizing large variations in toxicity of PCDD isomers were based on correlating the toxicity with lateral (2, 3, 7, and 8 positions) and longitudinal (1, 4, 6, and 9) patterns of substitutions, whereby the isomer specificities result, in particular equilibrium geometry, steric, and electric properties (polarizability).¹⁸ It was pointed out that twisting of the middle dioxin ring toward a boat conformation, which was speculated to be triggered by the longitudinal substitutions, markedly decreases the toxicity, presumably by diminishing the dioxins affinity toward binding to the target receptor.¹⁸ This may be the cause behind very small TEFs observed for 1,4,6,9-TCDD and OCDD, ~ 0.01 and < 0.0001 , respectively.⁹

A.2. Excited-State Geometries. Within a given symmetry the geometric parameters are changed in a strikingly similar fashion relative to the ground state in all three isomers. This indicates a formal equivalence of the corresponding excited states, and

TABLE 2: Angles (deg) Indicating the Extent of the Butterfly-like Folding in the Minima Structures of 1,4,6,9-TCDD and OCDD at the CASSCF(16,14)/cc-pVDZ Level


	1,4,6,9-TCDD	OCDD
α	169.8	169.6
β	159.9	159.4
γ	117.4	117.4

TABLE 3: Dominant Configurations in the CASSCF(16,14)/cc-pVDZ Wave Functions of 2,3,7,8-TCDD at the Optimized Geometries^a

state	singlets					triplets				
	b _{3u}	b _{1g}	b _{2g}	a _u	weight	b _{3u}	b _{1g}	b _{2g}	a _u	weight
A _g	2220	220	2200	200	0.785					
B _{3g}	2210	220	2200	210	0.805	2210	220	2200	210	0.553
						2220	210	2210	200	0.143
B _{2u}	2210	221	2200	200	0.331	2210	221	2200	200	0.443
	2220	220	2100	210	0.172	2221	210	2200	200	0.148
	2221	210	2200	200	0.121	2220	220	2100	210	0.113
B _{1u}	2210	220	2210	200	0.372	2221	220	2100	200	0.356
						2220	221	2200	100	0.282

^a Only configurations whose weight in the CI expansions is larger than 0.10.

hence it comes as no surprise that the ordering of the excitation energies and their relative differences are also quite similar in the three isomers (Section C). In comparison to the ground state, the C–O bond is shortened in the range of 0.010 (1¹B_{2u}) to 0.035 Å (1¹B_{3g}), with the sole exception of 1³B_{1u} where it is slightly elongated. Meanwhile, the C–C distances are generally increased in the range of 0.01 to 0.07 Å. Reduction in C–C distances is observed in three of the excited states: *r*_{3C–C} is reduced in 1¹B_{3g} and 1³B_{3g}, while 1³B_{1u} has both *r*_{1C–C} and *r*_{4C–C} shortened. The C–O–C angle is increased up to 3.4° (1¹B_{1u} of OCDD), whereas in 1³B_{1u} it is reduced by on average 1.5°. These occurrences are parallel to those in DD.³⁸

The singlet and triplet geometries within the same state symmetry exhibit analogous patterns of shortening and elongation of bonds relative to the ground state, the only exception being the B_{1u} state. From Table 3 it is seen that in 2,3,7,8-TCDD the leading terms in the CASSCF expansions are equivalent in the singlet and triplet states of the B_{3g} and B_{2u} symmetries, whereas the 1¹B_{1u} and 1³B_{1u} states differ largely in this respect, and hence the large discrepancies in their corresponding minimum structures. The analogous observations apply to the remaining two isomers. Consequently, on account of 1³B_{1u} dropping below 1³B_{2u}, the ordering of the triplet excitation energies differs from that of singlets, where 1¹B_{1u} is the highest lying of the first excited states (Section C).

B. Harmonic Wavenumbers. The CASSCF(16,14)/cc-pVDZ harmonic vibrational wavenumbers in the ground states (1¹A_g) of the three dioxins are given in Tables 4, 5, and 6. The harmonic wavenumbers of the lowest orbitally allowed excited states (1¹B_{2u}) are available as Supporting Information.

The calculated values are scaled by the factor of 0.9293, which minimizes the sum of squared differences between the

TABLE 4: CASSCF(16,14)/cc-pVDZ Harmonic Vibrational Wavenumbers (cm⁻¹) and Intensities (km mol⁻¹) in Parentheses of the Ground (1¹A_g) State of 2,3,7,8-TCDD^{a,b}

a _g		b _{1g}		b _{2g}	b _{3g}	
calcd	exptl	calcd	exptl	calcd	calcd	exptl
182	149	132		111	227	
253	206	352		278	387	383
556	548	430	441	578	536	
656	654	839	867	639	650	
748	739			814	998	985
1110	1100				1193	
1154	1236				1223	
1264	1284				1390	
1516	1442				1613	
1620	1600				3155	
3156						

a _u		b _{1u}		b _{2u}		b _{3u}	
calcd	calcd	exptl	calcd	exptl	calcd	exptl	
49	111		197		13		
214	322		440 (12)		450 (vw)	165	
575	495		678 (14)		864 (vw)	369	390
618	794 (37)	791 (w)	879 (196)		878 (s)	440	
809	939 (22)	938 (w)	1099 (13)		1107 (m)	841 (81)	890 (vw)
	1195 (62)	1176 (m)	1141 (197)		1270 (w)		
	1250 (48)	1330 (m)	1352 (308)		1306 (s)		
	1398 (35)	1393 (w)	1518 (1090)		1470 (vs)		
	1657		1585 (323)		1576 (m)		
	3155		3155				

^a The wavenumbers are scaled by the factor of 0.9293. ^b Experimental wavenumbers from refs 15 and 24.

TABLE 5: CASSCF(16,14)/cc-pVDZ Harmonic Vibrational Wavenumbers (cm⁻¹) and Intensities (km mol⁻¹) in Parentheses of the Ground (1¹A₁) State of 1,4,6,9-TCDD^{a,b}

a ₁		a ₂	b ₁		b ₂	
calcd	exptl	calcd	calcd	exptl	calcd	exptl
15		39	94		96	
97		173	217		188	
153		287	259		295	
291		441	327		415	
327		508	529		511	
430		575	700		518	
534		644	765		659	
622		646	976 (166)	965 (m)	686	
765 (55)	796 (w)	895	1107		894	
901		932	1141 (33)	1262 (w)	968 (256)	955 (m)
1118		1172	1289 (97)	1287 (m)	1211 (34)	1196 (w)
1141		1269	1506 (1110)	1456 (vs)	1229	
1253		1484	1597 (49)	1579 (w)	1494 (111)	1477 (m)
1475		1585	3155		1627 (8)	1612 (vw)
1628		3141			3141	
3155						

^a The wavenumbers are scaled by the factor of 0.9293. ^b Experimental wavenumbers from ref 15.

calculated and experimental wavenumbers in 2,3,7,8-TCDD, where the largest number of experimentally assigned modes is available. The vibrational modes of the ground state 1,4,6,9-TCDD and OCDD are given as symmetry species of the C_{2v} point group to which the true CASSCF minima belong (vide ante). In designating the modes, the molecule fixed coordinate system as in Figure 1 applies, and the symmetry species are consequently matched as follows: a₁ (a_g and b_{3u}), a₂ (b_{3g} and a_u), b₁ (b_{2g} and b_{1u}), and b₂ (b_{1g} and b_{2u}). In contrast, the 1¹B_{2u} states of all three isomers exhibit planar D_{2h} minima (please, refer to the Supporting Information). With the zero-point energy (ZPE) correction included, CASPT2-IPEA predicts 2,3,7,8-TCDD to be by 10.4 kJ mol⁻¹ (10.3 kJ mol⁻¹ with CASPT2-

TABLE 6: CASSCF(16,14)/cc-pVDZ Harmonic Vibrational Wavenumbers (cm⁻¹) and Intensities (km mol⁻¹) in Parentheses of the Ground (¹A_g) State of OCDD^{a,b}

a ₁		b ₁		b ₂	
calcd	calcd	calcd	exptl	calcd	exptl
7	33	64		77	
80	83	161		84	
159	181	217		181	
183	215	224		211	
225	317	332		331	
268	348	342		355	
335	543	459		451	
358	568	553		569	
551	632	837 (90)	841 (w)	650	
588	677	1014 (268)	999 (m)	661 (44)	664 (w)
746	740	1073 (35)	1110 (vw)	855 (108)	852 (w)
932	1027	1303 (2)	1336 (vw)	1005	
1104	1233	1488 (1360)	1425 (vs)	1232 (0.3)	1230 (vw)
1269	1408	1574 (284)	1550 (w)	1413 (162)	1400 (m)
1451	1568			1615	
1610					

^a The wavenumbers are scaled by the factor of 0.9293. ^b Experimental FT-IR spectrum from ref 27.

(*g*₂) more stable than the 1,4,6,9-isomer, which is comparable to the 12.1 kJ mol⁻¹ value at the B3LYP/cc-pVDZ level.

The exceedingly low (7–15 cm⁻¹) wavenumbers for the *b*_{3u}(*a*₁) butterfly mode are in line with previous investigations predicting an almost flat potential for the butterfly-like motion of the dioxin skeleton.^{25–28} Thus it comes as no surprise that the extra stabilization in the folded minima of 1,4,6,9-TCDD and OCDD is negligible relative to the *D*_{2h} saddle points. Likewise, the wavenumbers of the folded minima (Tables 5 and 6) deviate very slightly from those calculated at the planar geometries, with the difference in the ZPEs amounting to only 0.04 kJ mol⁻¹. Apart from the butterfly mode becoming real, noteworthy differences (up to 5 cm⁻¹) are found only within the *a*₁ (*a*_g and *b*_{3u}) set. In 1,4,6,9-TCDD these include an increase to 622 cm⁻¹ (from 617 cm⁻¹ in the saddle point) in the middle ring deformation mode along the *z* axis, and a decrease to 534 cm⁻¹ (from 538 cm⁻¹) in the side rings deformation mode along the *x* axis.

The applied scaling factor improves agreement with the experiment, enabling a clear-cut correspondence between the CASSCF and experimental wavenumbers, and an unambiguous assignment of vibrational modes. In 2,3,7,8-TCDD (Table 4) the largest relative deviations (up to 22%) are observed for the low-frequency modes of *a*_g and *b*_{2u} symmetry. However, quite similar flaws are seen with the SQM tailored B3LYP force field.²⁵ In general, the CASSCF wavenumbers and predicted intensities are close to those obtained via the B3LYP-SQM method,²⁵ which indicates a comparable reliability of the CASSCF and DFT force fields, e.g., by far the largest relative deviation (11%) between the two sets is observed for the skeleton vibration mode of *b*_{2u} symmetry (1141 cm⁻¹, Table 4). The B3LYP/cc-pVDZ wavenumbers are quite similar to those reported previously with use of the same functional and an another basis set of DZP quality.²⁸

As to the wavenumbers of 1,4,6,9-TCDD, here a relatively small number of vibrational modes is assigned, and the agreement with the experiment is similar to that for 2,3,7,8-TCDD (Table 5). The IR properties of the fully chlorinated isomer are comparatively less investigated, and in Table 6 an assignment is attempted based upon the FT-IR spectrum, IR active modes in the *D*_{2h} symmetry, and comparison between the calculated and observed²⁷ intensities.

A major feature in the IR spectra of the three dioxins is observed near 1500 cm⁻¹, where an extremely strong band resides corresponding to the *b*_{2u}(*b*₁) normal mode of the dioxin skeleton asymmetric stretching, which is strongly coupled to the CH bendings in the two tetrachlorinated isomers. The calculated intensities in the range of 1110 (2,3,7,8-TCDD) to 1360 km mol⁻¹ (OCDD) were attributed to an exceptionally strong in-phase coupling of the three fused rings.²⁵ In OCDD the corresponding band center undergoes a noteworthy red-shift of 30 cm⁻¹ (20 cm⁻¹) relative to 2,3,7,8-TCDD (1,4,6,9-TCDD), which can be rationalized in terms of an alleviated stretching of the more elongated (i.e., weaker) bonds of the OCDD skeleton, in line with the previous observations (Section A1). A characteristic splitting of this band observable in the spectra of some dioxins received considerable attention as a feature of analytical value.¹⁸ Whereas in 1,4,6,9-TCDD and OCDD the splitting occurs on account of the two near-lying modes of very strong and medium intensities (1506 and 1494 cm⁻¹ in 1,4,6,9-TCDD; 1488 and 1413 cm⁻¹ in OCDD; Tables 5 and 6), the band should remain intact in 2,3,7,8-TCDD, because no IR active mode sufficiently strong and close to the 1518 cm⁻¹ band can be confirmed theoretically (Table 4). Even so, in the FT-IR spectrum of 2,3,7,8-TCDD the band is clearly split,¹⁵ and consequently an involvement of Fermi resonance was proposed.²⁵

C. Electronic Transitions. The excitation energies of the singlet and triplet transitions are shown in Tables 7 and 8, respectively, and the oscillator strengths in the length representation are given in Table 9. The experimental UV absorption spectra,²⁰ supplemented by the vertical rules denoting the CASPT2-IPEA vertical band centers, are shown for 2,3,7,8-TCDD and OCDD in Figures 3 and 4, respectively. The TD-B3LYP method was also applied in the parent DD for a reference, and the results are available as Supporting Information.

According to the calculations, the far-UV spectra of the three dioxins should be well resolved into two basic band systems separated by a region of very low absorption. The first system contains low-intensity bands and is located in the 280–320 nm region. The second one spans the 200–240 nm region and contains the majority of allowed bands, some of which are very intense. These features are mainly confirmed in the experimental UV spectrum of 2,3,7,8-TCDD (Figure 3).²⁰ However, in case of OCDD a sensible comparison with experiment is much more difficult (Figure 4), because of the less favorable conditions under which the spectrum was recorded and higher temperatures involved. As a result, interesting features in the spectrum are largely obscured and the two regions are no longer nicely resolved as in the spectra of 2,3,7,8-TCDD,²⁰ 1,2,3,7,8-PCDD,²⁰ or DD.^{38,54} Relative to 2,3,7,8-TCDD, the equivalent transitions are irregularly shifted in 1,4,6,9-TCDD, but in OCDD each one is clearly red-shifted (Tables 7 and 8).

Preliminary tests, as well as comparison with the TD-B3LYP results, indicated that within the (16,14) π -active space, a total of 4 CASSCF roots in the *A*_g, 3 in the *B*_{1u} and *B*_{2u}, and 2 in the *B*_{3g} symmetry render a reasonably accurate description via the CASSCF/CASPT2 approach. It transpired that this set of roots comprises all of the most important states for describing the far-UV absorptions. The IPEA modification of the Fock operator produces on average 0.18 (in TCDDs) and 0.24 eV (in OCDD) higher singlet excitation energies than the *g*₂ modification (Table 7), whereas for the triplets these are much more similar (Table 8). The smallest discrepancies between the two approaches are observed for the 2¹A_g state (0.08 eV) and the largest ones for

TABLE 7: Singlet Excitation Energies (vertical T_v and Adiabatic T_0 in eV) at the CASPT2(16,14)/cc-pVDZ and TD-B3LYP/cc-pVDZ Levels

state	2,3,7,8-TCDD					1,4,6,9-TCDD					OCDD				
	CASPT2				TD-B3LYP	CASPT2				TD-B3LYP	CASPT2				TD-B3LYP
	g_2^a		IPEA ^b			g_2^a		IPEA ^b			g_2^a		IPEA ^b		
	T_v	T_0	T_v	T_0	T_v	T_0	T_v	T_0	T_v	T_0	T_v	T_0	T_v	T_0	T_v
1 ¹ B _{3g}	3.90	3.79	4.12	3.96	3.99	3.89	3.77	4.07	3.92	4.03	3.72	3.62	3.93	3.80	3.88
1 ¹ B _{2u}	4.06	3.93	4.14	4.01	4.22	4.08	4.00	4.18	4.08	4.32	3.86	3.79	3.99	3.91	4.11
2 ¹ A _g	4.28		4.35		4.31	4.36		4.44		4.51	4.19		4.29		4.28
1 ¹ B _{3u}					4.91					5.04					4.19
1 ¹ B _{1g}					5.10					5.49					4.50
2 ¹ B _{2u}	5.27		5.47		5.19	5.29		5.50		5.00	4.95		5.21		4.77
1 ¹ B _{1u}	5.54	5.40	5.82	5.69	5.26	5.66	5.63	5.91	5.85	5.23	5.30	5.22	5.65	5.53	5.04
3 ¹ B _{2u}	5.83		6.05		5.69	5.77		6.04		6.15	5.38		5.70		5.57
2 ¹ B _{1u}	5.85		6.00		5.46	5.75		5.95		5.51	5.47		5.71		5.17
3 ¹ A _g	6.26		6.44		5.39	6.44		6.59		5.29	6.15		6.36		5.07
3 ¹ B _{1u}	6.67		6.93		5.78	6.55		6.81		5.76	6.19		6.54		5.39
1 ¹ B _{2g}					5.92					5.53					4.72
1 ¹ A _u					6.06					5.77					4.91
4 ¹ A _g	6.78		6.94		6.07	6.84		7.01		5.86	6.52		6.76		5.47
2 ¹ B _{3g}	6.82		7.01		5.60	7.03		7.14		5.25	6.59		6.80		5.05

^a The g_2 modification of the Fock operator combined with the imaginary level shift parameter of 0.20 hartree. ^b The IPEA level shift parameter of 0.10 hartree combined with the imaginary level shift parameter of 0.20 hartree.

TABLE 8: Triplet Excitation Energies (vertical T_v and Adiabatic T_0 in eV) at the CASPT2(16,14)/cc-pVDZ and TD-B3LYP/cc-pVDZ Levels

state	2,3,7,8-TCDD					1,4,6,9-TCDD					OCDD				
	CASPT2				TD-B3LYP	CASPT2				TD-B3LYP	CASPT2				TD-B3LYP
	g_2^a		IPEA ^b			g_2^a		IPEA ^b			g_2^a		IPEA ^b		
	T_v	T_0	T_v	T_0	T_v	T_0	T_v	T_0	T_v	T_0	T_v	T_0	T_v	T_0	T_v
1 ³ B _{3g}	3.34	2.96	3.46	3.11	3.02	3.33	3.01	3.43	3.13	3.06	3.16	2.82	3.30	2.98	2.91
1 ³ A _g	3.76	3.56	3.89	3.70	3.55	3.96	3.83	4.11	3.98	3.86	3.73	3.59	3.91	3.77	3.65
1 ³ B _{1u}	3.84	3.74	3.92	3.80	3.54	3.86	3.60	3.94	3.70	3.55	3.70	3.47	3.80	3.59	3.38
1 ³ B _{2u}	3.84	3.64	3.97	3.78	3.64	3.93	3.82	4.08	3.97	3.88	3.71	3.59	3.89	3.78	3.67
2 ³ B _{3g}	4.06		4.17		4.12	3.99		4.10		3.95	3.86		3.99		3.79
2 ³ B _{1u}	4.34		4.45		4.32	4.37		4.48		4.35	4.19		4.32		4.09
2 ³ B _{2u}	4.94		5.11		4.57	4.64		4.80		4.15	4.51		4.73		4.04
1 ³ B _{3u}					4.68					4.81					4.01
1 ³ B _{1g}					4.86					5.37					4.32
2 ³ A _g	5.18		5.35		4.96	4.99		5.14		4.44	4.81		5.03		4.35
3 ³ B _{2u}	5.65		5.80		5.13	5.81		6.01		5.40	5.40		5.63		
3 ³ A _g	5.78		5.92		5.18	5.75		5.93		5.55	5.42		5.60		4.35
3 ³ B _{3g}	6.05		6.21		5.63	6.09		6.22		5.35	5.80		6.01		5.16
3 ³ B _{1u}	6.87		6.99		5.10	6.88		7.00		5.30	6.64		6.83		5.00
1 ³ A _u										5.36					4.62
1 ³ B _{2g}					5.72					5.22					4.48

^a The g_2 modification of the Fock operator combined with the imaginary level shift parameter of 0.20 hartree. ^b The IPEA level shift parameter of 0.10 hartree combined with the imaginary level shift parameter of 0.20 hartree.

TABLE 9: CASSCF/cc-pVDZ and TD-B3LYP/cc-pVDZ Oscillator Strengths in the Length Representation

	2,3,7,8-TCDD		1,4,6,9-TCDD		OCDD	
	CASSCF ^a	TD-B3LYP	CASSCF ^a	TD-B3LYP	CASSCF ^a	TD-B3LYP
1B _{2u} ← A _g	1.34 × 10 ⁻²	1.47 × 10 ⁻¹	6.28 × 10 ⁻³	6.30 × 10 ⁻³	7.70 × 10 ⁻³	3.00 × 10 ⁻²
1B _{1u} ← A _g	8.49 × 10 ⁻³	1.20 × 10 ⁻³	7.27 × 10 ⁻⁶	5.84 × 10 ⁻²	1.37 × 10 ⁻³	3.22 × 10 ⁻²
1B _{3u} ← A _g		0		1.80 × 10 ⁻³		1.00 × 10 ⁻⁴
2B _{2u} ← A _g	4.03 × 10 ⁻¹	4.83 × 10 ⁻¹	4.85 × 10 ⁻¹	6.80 × 10 ⁻¹	4.75 × 10 ⁻¹	8.75 × 10 ⁻¹
2B _{1u} ← A _g	3.71 × 10 ⁻²	2.70 × 10 ⁻³	1.18 × 10 ⁻¹	4.50 × 10 ⁻³	8.28 × 10 ⁻²	0
3B _{2u} ← A _g	9.60 × 10 ⁻¹	9.77 × 10 ⁻¹	8.56 × 10 ⁻¹	8.20 × 10 ⁻³	8.78 × 10 ⁻¹	2.45 × 10 ⁻¹
3B _{1u} ← A _g	9.01 × 10 ⁻³	1.75 × 10 ⁻¹	2.77 × 10 ⁻³	2.98 × 10 ⁻¹	2.91 × 10 ⁻⁴	1.09 × 10 ⁻²

the 1¹B_{1u} state (0.29 eV). If the IPEA level shift is reduced further down to 0.05 hartree, the average differences diminish to within 0.10 eV. The CASPT2(g_2) results are much closer to the ones obtained without any modification of the Fock operator. Of the two differently styled CASPT2 approaches, a slight advantage should probably be given to IPEA, whereby the vertical band centers are positioned more in accord with the experimentally observable absorption patterns. Because no high-

resolution electron spectra of the three dioxins have been published, this is the most that can be presently said on the relative performance of the two approaches in this case. For this reason, the vertical rules in Figures 3 and 4 are chosen to mark the positions of the CASPT2-IPEA vertical transitions.

Because the CASSCF active orbitals are easily identifiable among the Kohn–Sham (KS) orbitals, the excitations that make dominant contributions to the π – π^* excited states are straight-

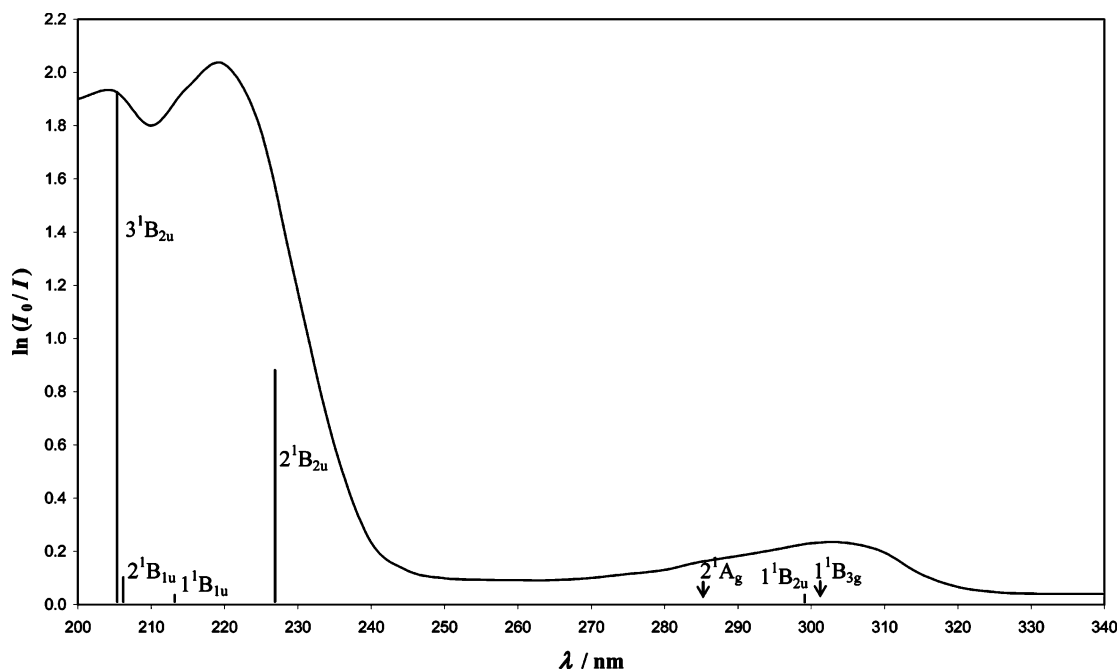


Figure 3. The calculated (CASPT2-IPEA/cc-pVDZ vertical energies from Table 7) and experimental (185 °C, ref 20) UV absorption spectrum of 2,3,7,8-TCDD. Oscillator strengths are roughly indicated (Table 9) by the relative height of the vertical rules. Orbitally forbidden transitions are indicated by the arrows.

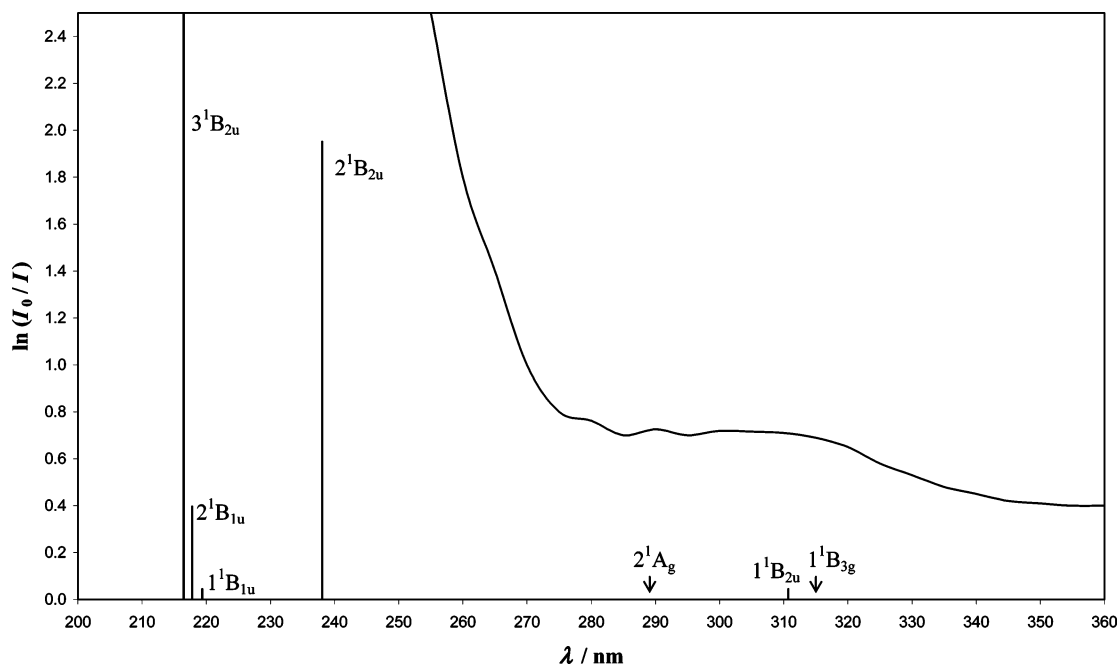


Figure 4. The calculated (CASPT2-IPEA/cc-pVDZ vertical energies from Table 7) and experimental (275 °C, ref 20) UV absorption spectrum of OCDD. Oscillator strengths are roughly indicated (Table 9) by the relative height of the vertical rules. Orbitally forbidden transitions are indicated by the arrows.

forward to compare between the two methods. These contributions are nearly identical, which confirms that equivalent excited states are described by CASSCF and TD-B3LYP. The corresponding excitation energies are in good agreement for the few low-lying excited states in the region of the first band system (Tables 7 and 8). The agreement deteriorates for the transitions contributing to the second band system, where the TD-B3LYP energies are red-shifted by 0.05–0.40 eV relative to the CASPT2(g_2) ones. Judging from the band positions in the UV spectra of 2,3,7,8-TCDD and DD^{20,38,54} (please refer also to the Supporting Information), these values are more or less underestimated. Toward even higher excited states the reliability of TD-B3LYP declines rapidly on account of progressively more

underestimation of the excitation energies. Thus the most significant deviation from CASPT2 occurs with the high-lying 2^1B_{3g} and 3^3B_{1u} states, whose TD-B3LYP excitation energies must already be grossly underestimated (around 1.2–1.8 eV) in all three isomers as well as in the parent DD. The $-\epsilon_{\text{HOMO}}$ energies, which were suggested as a criterion in estimating the reliability threshold within TD-DFT approaches,⁵⁵ equal 6.08 eV in 2,3,7,8-TCDD, 6.24 eV in 1,4,6,9-TCDD, and 6.49 eV in OCDD. In this case these values seem to be a fairly good estimate of the upper bound of the region where TD-B3LYP starts performing relatively poorly. Additional problems with the TD-DFT based approaches in the case of dioxins might be posed by the pronounced multiconfigurational nature of PCCDs.

Although the numerical discrepancies between the CASSCF and TD-B3LYP oscillator strengths are for the most part notable (Table 9), certain similar trends are also shown. Thus, the $1^1B_{2u} \leftarrow 1^1A_g$ transition, which provides the main contribution to the 280–320 nm region, is considerably attenuated in 1,4,6,9-TCDD and OCDD relative to 2,3,7,8-TCDD. The nearby $2^1A_g \leftarrow 1^1A_g$ may become visible in the butterfly folded geometries, or likewise via the vibronic coupling with the butterfly mode. In the folded minima of 1,4,6,9-TCDD and OCDD the TD-B3LYP oscillator strength of the equivalent transition is on the order of 10^{-4} . It was conjectured that the $1^1B_{2u} \leftarrow 1^1A_g$ and $2^1A_g \leftarrow 1^1A_g$ bands may be solely responsible for the absorption patterns in the first region.³⁸ Compared to DD,³⁸ the structure of high-intensity absorption bands in the 200–240 nm region becomes more complex because of the presence of additional transition ($3^1B_{2u} \leftarrow 1^1A_g$) with by far the largest CASSCF oscillator strength in all three isomers (Table 9). The TD-B3LYP oscillator strengths are here more erratic, altering the largest intensity between $2^1B_{2u} \leftarrow 1^1A_g$ and $3^1B_{2u} \leftarrow 1^1A_g$, and also assigning a considerable one to $3^1B_{1u} \leftarrow 1^1A_g$. The wavelengths of peak absorptions were measured in the two regions and found to be very similar for 2,3,7,8-TCDD and OCDD.²⁰ The experimental values of 4.09 eV (4.06 eV) for the first region in 2,3,7,8-TCDD (OCDD) are in a very good agreement with the vertical excitation energies for the 1^1B_{2u} state, whereas the peak absorption in the second region (5.55 eV) is roughly halfway between the 2^1B_{2u} and 3^1B_{2u} band centers. The peak emissions from the laser-induced fluorescence²⁰ were observed at 3.70 eV (3.16 eV), and are red-shifted relative to the calculated $1^1B_{2u} \leftarrow 1^1A_g$ adiabatic excitation energies. Because in OCDD this red shift is suspiciously large compared to that of 2,3,7,8-TCDD, a possibility of fast singlet–triplet conversion in OCDD was suggested.²⁰

The set of KS virtual orbitals include two σ^* type orbitals of a_g and b_{2u} symmetry, which being rather low-lying disrupt the π^* sequence in all three dioxins. The presence of these orbitals brings about some additional transitions of the $\pi-\sigma^*$ type that cannot be described within the CASSCF/CASPT2 approach. These yield the B_{3u} , B_{1g} , B_{2g} , and A_u states (Tables 7 and 8). The lowest lying of them, the B_{3u} state, is also the only one that is orbitally allowed within the D_{2h} point symmetry, although being x polarized it acquires only a small intensity (Table 9). The effects of the butterfly-like relaxation on the excitation energies and oscillator strengths were estimated by carrying out the TD-B3LYP calculations in the CASSCF folded minima of 1,4,6,9-TCDD and OCDD. Whereas the $\pi-\pi^*$ transitions undergo very small changes in both these parameters, all $\pi-\sigma^*$ transitions are invariably blue-shifted by ~ 0.1 eV. The states equivalent to $1B_{1g}$ and $1B_{2g}$ acquire finite oscillator strengths, noteworthy of which are only $1B_{2g}$ of 1,4,6,9-TCDD ($f = 4 \times 10^{-3}$) and $1B_{1g}$ of OCDD ($f = 2 \times 10^{-3}$). The appearance of the OCDD spectrum, in particular within larger folding amplitudes, may be affected by the $1B_{1g}$ equivalent state, because it is expected in the region of lower absorption (~ 273 nm), whereas the B_{2g} equivalent state in 1,4,6,9-TCDD (~ 220 nm) remains essentially covered by the most intense bands.

The lowest triplet states of the polychlorinated dioxins were assigned on basis of the vibration structure in the low-temperature Shpol'skii phosphorescence spectra.²¹ Contrary to DD, where the key features are the barely visible 0–0 origin and 1^3B_{3g} the lowest transition,^{22,38} high-intensity 0–0 origins and the vibration structure matching the totally symmetrical modes pointed at 1^3B_{1u} as the lowest triplet in 2,3,7,8-TCDD and OCDD.²¹ However, neither of the used theoretical ap-

proaches verified this (Table 8). Even though the triplet and singlet B_{1u} states differ largely in origin (Section A2), whereby 1^3B_{1u} is considerably lowered, this is not sufficient to drop 1^3B_{1u} below 1^3B_{3g} . In fact both CASPT2 and TD-B3LYP place 1^3B_{1u} nowhere near the 1^3B_{3g} state—it is on average more than 0.5 eV above. The previous studies (INDO and CNDO-CIS in 2,3,7,8-TCDD) also yielded 1^3B_{3g} as the lower of the two, but as the 1^3B_{1u} state was placed within 1000 cm^{-1} of 1^3B_{3g} , it was assumed that the order of the two states was predicted incorrectly.²⁴ All the same, the CASPT2 and TD-DFT excitation energies for the 1^3B_{3g} state are in very good agreement with the alleged 0–0 origins, 3.03 (410 nm) and 2.96 eV (419 nm) for 2,3,7,8-TCDD and OCDD, respectively.²¹ Furthermore, the three chlorinated isomers appear completely analogous to the parent DD in this respect.³⁸ The puzzle thus remains unresolved, but the convincing theoretical predictions in favor of 1^3B_{3g} at least call for caution in definitely assigning the lowest triplet to 1^3B_{1u} in 2,3,7,8-TCDD and OCDD.

Conclusions

We have presented the CASSCF/CASPT2 and DFT-B3LYP (TD-B3LYP) calculations of structure, harmonic vibrational frequencies, and electronic spectra of three dioxin isomers (2,3,7,8-TCDD, 1,4,6,9-TCDD, and OCDD). In the CASSCF calculations active spaces consisted of 16 electrons distributed in 14 active orbitals, which corresponds to the full space of π orbitals on C and O atoms. The use of the relatively small basis set (cc-pVDZ) was imposed by the size of the system, as well as the large active spaces employed, which are very close to the present day limit. Resorting to the imaginary level shift (ILS)⁴¹ technique proved necessary throughout to eliminate the singularities due to intruder states. The performances of the IPEA⁴⁴ and g_2 ⁴³ modifications of the Fock operator in CASPT2 were compared. The CASPT2 excitation energies calculated with the IPEA level shift⁴⁴ parameter of 0.10 hartree combined with the ILS parameter of 0.20 hartree seem to be the most trustworthy results. The TD-B3LYP method performs well in describing the lower excited states, but toward the 6.0 eV threshold tends to increasingly underestimate the excitation energies. This threshold complies well with the $-\epsilon_{\text{HOMO}}$ criterion.⁵⁵

Whereas the B3LYP geometric optimizations result in the D_{2h} planar minima in all three isomers, the CASSCF predict slightly butterfly-folded minima of C_{2v} symmetry in 1,4,6,9-TCDD and OCDD. Although such a possibility was anticipated earlier,¹⁸ the folded minima have not until now been verified theoretically. The folding mitigates somewhat the repulsion between the O atoms and longitudinal chlorine substituents, although the extra stabilization ends up exceedingly small, presumably on account of the less pronounced stabilization via the π electron delocalization. The consequences on the vibrational and electronic spectra are shown to be minor, but the folding tendencies may still be partly responsible for the negligible toxic equivalence factors of 1,4,6,9-TCDD and OCDD.⁹

The CASSCF(16,14) and DFT force fields are observed to be of a comparable reliability. In the case of the two tetrachlorinated isomers the deviations of the CASSCF wavenumbers and IR intensities from those derived from the B3LYP-SQM tailored force field²⁵ are generally small. Thus the CASSCF method may equally provide the means of assigning the IR spectra and distinguishing between the isomers. In addition, the most prominent bands in the IR spectra of OCDD²⁷ were assigned on the basis of a good agreement with the CASSCF wavenumbers and intensities.

The CASPT2 and TD-B3LYP excitation energies indicate that the electron spectra of the three dioxins are well resolved into two regions separated by a region of low absorption. The first region around 280–320 nm is of relatively low intensity. Here the main contributions can be attributed to the $1^1B_{2u} \leftarrow 1^1A_g$ transition and possibly the vibronically allowed $2^1A_g \leftarrow 1^1A_g$ transition. The second region around 200–240 nm contains the most intense bands, and is dominated by the $2^1B_{2u} \leftarrow 1^1A_g$ and $3^1B_{2u} \leftarrow 1^1A_g$ transitions with by far the largest oscillator strengths. A set of complementary states of the $\pi-\sigma^*$ type (B_{3u} , B_{1g} , B_{2g} , A_u) was provided by the TD-B3LYP approach, but the corresponding transitions are generally of modest intensities. The B_{1g} and B_{2g} states are of some interest, because they gain intensity via the vibronic coupling with the butterfly flapping mode, or become orbitally allowed in the C_{2v} butterfly minima of 1,4,6,9-TCDD and OCDD. However, within folding amplitudes similar to those of the CASSCF minima, the latter effect is predicted to be small.

Both theoretical approaches convincingly predict 1^3B_{3g} as the lowest triplet state in all three isomers, which contradicts the experimental assignment (1^3B_{1u}).²² Apart from that, the calculated IR and UV spectral properties agree well with experiment, and appear sufficiently distinct to allow for an unambiguous identification of the three isomers.

Acknowledgment. This work was supported by the Ministry of Science and Technology of the Republic of Croatia under project number 0098033.

Supporting Information Available: A pictorial representation of the Kohn–Sham orbitals and (16,14) active space in 2,3,7,8-TCDD, tables of the harmonic vibrational wavenumbers in the 1^1B_{2u} excited state of all three isomers, as well as the TD-B3LYP calculation on the excited states of dibenzo-*p*-dioxin (DD). This material is available free of charge via the Internet at <http://pubs.acs.org>.

References and Notes

- (1) (a) *Sax's Dangerous Properties of Industrial Materials*, 10th ed.; Lewis, R. J., Sr., Ed.; John Wiley & Sons: New York, 2000; Vols. 1–3. (b) Shepard, B. M.; Young, A. L. In *Human and Environmental Risks of Chlorinated Dioxins and Related Compounds*; Tucker, R. E., Young, A. L., Gray, A. P., Eds.; Plenum Press: New York, 1983.
- (2) Atkinson, R. Atmospheric chemistry of PCBs, PCDDs, and PCDFs. In *Chlorinated Organic Micropollutants: Issues in Environmental Science and Technology*; Hester, R. E., Harrison, R. M., Eds.; The Royal Society of Chemistry: Cambridge, UK, 1996.
- (3) Baker, J. I.; Hites, R. A. *Environ. Sci. Technol.* **2000**, *34*, 2879.
- (4) Rappe, C. *Pure Appl. Chem.* **1996**, *68*, 1781.
- (5) Rappe, C.; Öberg, L. G.; Andersson, R. *Organohalogen Compd.* **1999**, *43*, 249.
- (6) Sabljic, A. *Chemosphere* **2001**, *43*, 363.
- (7) Fuster, G.; Schumacher, M.; Domingo, J. L. *Environ. Sci. Pollut. Res. Int.* **2002**, *9*, 241.
- (8) Kociba, R. J.; Cabey, O. *Chemosphere* **1985**, *14*, 649.
- (9) Van den Berg M.; Birnbaum L.; Bosveld A. T. C.; Brunström B.; Cook P.; Feeley M.; Giesy J. P.; Hanberg A.; Hasegawa R.; Kennedy S. W.; Kubiak, T.; Larsen, J. C.; van Leeuwen F. X.; Liem, A. K. D.; Nolt, C.; Peterson, R. E.; Poellinger, L.; Safe, S.; Schrenk, D.; Tillitt, D.; Tysklind, M.; Younes, M.; Wærn, F.; Zacharewski, T. *Environ. Health Perspect.* **1998**, *106*, 775.
- (10) Williamson, M. A.; Gasiewicz, T. A.; Opanashuk, L. A. *Toxicol. Sci.* **2005**, *83*, 340.
- (11) Grassman, J. A.; Masten, S. A.; Walker, N. J.; Lucier, G. W. *Environ. Health Perspect.* **1998**, *106*, 761.
- (12) Poland, A.; Knutson, J. C. *Annu. Rev. Pharmacol. Toxicol.* **1982**, *22*, 517.
- (13) (a) Schutte, C. J. H.; Bertie, J. E.; Bunker, P. R.; Hougen, J. T.; Mills, I. M.; Watson, J. K. G.; Winnewisser, B. P. *Pure Appl. Chem.* **1997**, *69*, 1633. (b) Schutte, C. J. H.; Bertie, J. E.; Bunker, P. R.; Hougen, J. T.; Mills, I. M.; Watson, J. K. G.; Winnewisser, B. P. *Pure Appl. Chem.* **1997**, *69*, 1641.

- (14) Gurka, D. F.; Billets, S.; Brasch, J. W.; Riggle, C. J. *Anal. Chem.* **1985**, *57*, 1975.
- (15) Gurka, D. F.; Brasch, J. W.; Barnes, R. H.; Riggle, C. J.; Bourne S. *Appl. Spectrosc.* **1986**, *40*, 978.
- (16) Wurrey, C. J.; Bourne, S.; Kleopfer, R. D. *Anal. Chem.* **1986**, *58*, 483.
- (17) Grainger, J.; Gelbaum, L. T. *Appl. Spectrosc.* **1987**, *41*, 809.
- (18) Grainger, J.; Reddy, V. V.; Patterson, D. G., Jr. *Appl. Spectrosc.* **1988**, *42*, 643.
- (19) Khasawneh, I. M.; Winefordner, J. D. *Talanta* **1988**, *35*, 267.
- (20) Funk, D. J.; Oldenborg, R. C.; Dayton, D.-P.; Lacosse, J. P.; Draves, J. A.; Logan, T. J. *Appl. Spectrosc.* **1995**, *49*, 105.
- (21) Klimenko, V. G.; Nurmukhametov, R. N. *J. Fluoresc.* **1998**, *8*, 129.
- (22) Klimenko, V. G.; Nurmukhametov, R. N.; Gastilovich, E. A. *Opt. Spectrosc.* **1997**, *83*, 92.
- (23) Gastilovich, E. A.; Serov, S. A.; Korol'kova, N. V.; Klimenko, V. G. *J. Mol. Struct.* **2000**, *553*, 243.
- (24) Gastilovich, E. A.; Klimenko, V. G.; Korol'kova, N. V.; Rauhut, G. *Chem. Phys.* **2001**, *270*, 41.
- (25) Rauhut, G.; Pulay, P. *J. Am. Chem. Soc.* **1995**, *117*, 4167.
- (26) Fujii, T.; Tanaka, K.; Tokiwa, H.; Soma, Y. *J. Phys. Chem.* **1996**, *100*, 4810.
- (27) Sommer, S.; Kamps, R.; Schumm, S.; Kleinermanns, K. F. *Anal. Chem.* **1997**, *69*, 1113.
- (28) Mhin, B. J.; Choi, J.; Choi, W. *J. Am. Chem. Soc.* **2001**, *123*, 3584.
- (29) Lee, J. E.; Choi, W.; Mhin, B. J.; Balasubramanian, K. *J. Phys. Chem. A* **2004**, *108*, 607.
- (30) (a) Wratten, R. J.; Ali, M. A. *Mol. Phys.* **1967**, *13*, 233. (b) Colonna, F. P.; Distefano, G.; Galasso, V.; Irgolic, K. J.; King, C. E.; Pappalardo, G. C. *J. Organomet. Chem.* **1978**, *146*, 235. (c) Baldo, M.; Irgolic, K. J.; Nicolini, M.; Pappalardo, G. C.; Viti, V. *J. Chem. Soc., Faraday Trans. 2* **1983**, *79*, 1633.
- (31) Baba, M.; Doi, A.; Tatamitani, Y.; Kasahara, S.; Katô, H. *J. Phys. Chem. A* **2004**, *108*, 1388.
- (32) Hirokawa, S.; Imasaka, T.; Urakami, Y. *J. Mol. Struct. THEOCHEM* **2003**, *622*, 229.
- (33) Andersson, K.; Malmqvist, P.-Å.; Roos, B. O. *J. Chem. Phys.* **1992**, *96*, 1218.
- (34) Roos, B. O.; Andersson, K.; Fülcher, M. P.; Serrano-Andrés, L.; Pierloot, K.; Merchán, M.; Molina, V. *J. Mol. Struct. THEOCHEM* **1996**, *388*, 257.
- (35) Runge, E.; Gross, E. K. U. *Phys. Rev. Lett.* **1994**, *52*, 997.
- (36) Roos, B. O. Multiconfigurational (MC) Self-Consistent Field (SCF) Theory. In *European Summerschool in Quantum Chemistry*, Book II; Roos, B. O., Widmark, P.-O., Eds.; Lund University: Lund, 2000; pp 285–360.
- (37) (a) Becke, A. D. *J. Chem. Phys.* **1993**, *98*, 5648. (b) Lee, C.; Yang, W.; Parr, R. G. *Phys. Rev.* **1988**, *B41*, 785.
- (38) Ljubić, I.; Sabljic, A. *J. Phys. Chem. A* **2005**, *109*, 8209.
- (39) Schaftenaar, G.; Noordik, J. H. *J. Comput.-Aided Mol. Des.* **2000**, *14*, 123.
- (40) Roos, B. O. In *Advances in Chemical Physics: Ab Initio Methods in Quantum Chemistry II*; Lawley, K. P., Ed.; Wiley: New York, 1987; p 399.
- (41) Forsberg, N.; Malmqvist, P.-Å. *Chem. Phys. Lett.* **1997**, *274*, 196.
- (42) Roos, B. O.; Andersson, K. *Chem. Phys. Lett.* **1995**, *245*, 215.
- (43) Andersson, K. *Theor. Chim. Acta* **1995**, *91*, 31.
- (44) Ghigo, G.; Roos, B. O.; Malmqvist, P.-Å. *Chem. Phys. Lett.* **2004**, *396*, 142.
- (45) Dunning, T. H. *J. Chem. Phys.* **1989**, *90*, 1007.
- (46) Karlström, G.; Lindh, R.; Malmqvist, P.-Å.; Roos, B. O.; Ryde, U.; Veryazov, V.; Widmark, P.-O.; Cossi, M.; Schimmelpfennig, B.; Neogrady, P.; Seijo, L. *Comput. Mater. Sci.* **2003**, *28*, 222.
- (47) Frisch, M. J.; Trucks, G. W.; Schlegel, H. B.; Scuseria, G. E.; Robb, M. A.; Cheeseman, J. R.; Montgomery, J. A., Jr.; Vreven, T.; Kudin, K. N.; Burant, J. C.; Millam, J. M.; Iyengar, S. S.; Tomasi, J.; Barone, V.; Mennucci, B.; Cossi, M.; Scalmani, G.; Rega, N.; Petersson, G. A.; Nakatsuji, H.; Hada, M.; Ehara, M.; Toyota, K.; Fukuda, R.; Hasegawa, J.; Ishida, M.; Nakajima, T.; Honda, Y.; Kitao, O.; Nakai, H.; Klene, M.; Li, X.; Knox, J. E.; Hratchian, H. P.; Cross, J. B.; Bakken, V.; Adamo, C.; Jaramillo, J.; Gomperts, R.; Stratmann, R. E.; Yazyev, O.; Austin, A. J.; Cammi, R.; Pomelli, C.; Ochterski, J. W.; Ayala, P. Y.; Morokuma, K.; Voth, G. A.; Salvador, P.; Dannenberg, J. J.; Zakrzewski, V. G.; Dapprich, S.; Daniels, A. D.; Strain, M. C.; Farkas, O.; Malick, D. K.; Rabuck, A. D.; Raghavachari, K.; Foresman, J. B.; Ortiz, J. V.; Cui, Q.; Baboul, A. G.; Clifford, S.; Cioslowski, J.; Stefanov, B. B.; Liu, G.; Liashenko, K.; Piskorz, P.; Komaromi, I.; Martin, R. L.; Fox, D. J.; Keith, T.; Al-Laham, M. A.; Peng, C. Y.; Nanayakkara, A.; Challacombe, M.; Gill, P. M. W.; Johnson, B.; Chen, W.; Wong, M. W.; Gonzalez, C.; Pople, J. A. *Gaussian 03*, revision C.02; Gaussian, Inc.: Wallingford, CT, 2004.
- (48) Malmqvist, P.-Å.; Roos, B. O. *Chem. Phys. Lett.* **1989**, *155*, 189.
- (49) Boer, F. P.; van Remoortere, F. P.; North, P. P.; Neuman, M. A. *Acta Crystallogr.* **1972**, *B28*, 1023.

(50) Neuman, M. A.; North, P. P.; Boer, F. P. *Acta Crystallogr.* **1972**, *B28*, 2313.

(51) Bernhardsson, A.; Forsberg, N.; Malmqvist, P.-Å.; Roos, B. O.; Serrano-Andrés, L. *J. Chem. Phys.* **2000**, *112*, 2798.

(52) The data were taken from the Computational Chemistry Comparison and Benchmark DataBase (<http://srdata.nist.gov/cccbdb/>), a public service provided by the National Institute of Standards and Technology (NIST).

(53) (a) Torelli, T.; Mitas, L. *Phys. Rev. Lett.* **2000**, *85*, 1702. (b) Majumder, C.; Briere, T.; Mizuseki, H.; Kawazoe, Y. *J. Phys. Chem. A* **2002**, *106*, 7911.

(54) Ryzhikov, M. B.; Rodionov, A. N.; Stepanov, A. N. *Zh. Fiz. Khim.* **1989**, *63*, 2125 (in Russian).

(55) Casida, M. E.; Jamorski, C.; Casida, K. C.; Salahub, D. R. *J. Chem. Phys.* **1998**, *108*, 4439.